Practical Techniques for Measuring MEMS Properties

J. V. Clark, D. Garmire, M. Last, J. Demmel, S. Govindjee

University of California at Berkeley, Berkeley, CA, USA, jvclark@eecs.berkeley.edu

ABSTRACT

We propose practical analysis techniques to accurately measure geometric, dynamic, and material properties of MEMS. Analytical methods and test structures are presented to extract over a dozen properties by electric probing in a minimal chip area. Geometric properties include fabrication error with respect to layout geometry such as beam widths, gap spacings, etch holes, and beam lengths. Dynamic properties include mass, damping, stiffness, bulk compliance, quality factor, exponential damping factor, displacement amplitude, velocity amplitude, comb drive force, and fringing field factor. Material properties include Young's modulus, residual stress, shear modulus, Poisson's ratio, and material density. These techniques differ from those currently available in practicality and that no geometric, dynamic, or material property values are presumed. Only capacitively-based measurements are required.

Keywords: property extraction, characterization, metrology

1 INTRODUCTION

Although microsystems technology is becoming a well-established industry, testing standards for MEMS properties are still under development. S. Brown [1] states that the industry has suffered due to an absence of standard testing methods, making it difficult for manufacturers to specify their materials and for customers to specify their needs. J. Marshall [2] states that industrially accepted standards are necessary to facilitate international commerce. Just recently, the first three MEMS testing standards were offered by the National Institute of Standards and Technology (NIST) and the American Society for Testing and Materials (ASTM) for beam length and residual stress [2]. A difficultly in developing MEMS testing standards is due to the numerous uncertain properties of MEMS. These uncertainties may cause testing methods to yield only a couple of significant digits of accuracy, and different methods can yield different results [7]. Additionally, microscale properties are extremely sensitive to process variations. Accuracy and precision of standard processes are difficult to control – properties vary by recipe, fabrication run, wafer-to-wafer, and across the wafer.

Although there are few testing standards, there are plenty of nonstandard testing methods available in the MEMS literature. Most methods are expensive with respect to cost and time, which make them nonideal for a competitive industry. Most methods inevitably rely on unconfirmed properties, which reduce confidence in the results. Examples of previous efforts include full chips of test arrays [3-4], vacuum chambers to reduce damping [5], scanning electron microscopy for geometry [7], large structures or highly specialized equipment for stress [2, 6], and FEA-based geometrical extraction [11]. W. Sharpe Jr. provides an extensive overview [7]. Due to the impracticality of most methods, properties are often coarsely measured, or presumed from the literature. The properties of a device are typically left as roughly-known, and the device is electronically tuned for good performance. Although electronic tuning has worked well for getting simple systems to market quickly, progress toward practical and accurate measurement techniques has been slow. Measurements of fundamental properties are critical to the study of complex phenomena, and to the improved modeling and prediction of more complex microsystems.

To address the above issues, we propose practical analysis techniques which do not rely on presumed properties. Our techniques differ from previous work as follows. Instead of obtaining one to three properties from large arrays of structures, we obtain over a dozen properties from small test sets. We refine the numerous uncertainties by deducing fundamental properties through measurement. For precision, measurements are based on capacitance [10], which is the most sensitive type of sensing to date. As an exceptional example, capacitive changes on the order of zeptofarads from the deflection of beams that have displaced a few femtometers have been reported [12]. We also identify the first use of velocity resonance in MEMS as a substitute for resonance in vacuum. The following sections provide the theoretical basis and formulas for property measurements.

2 FABRICATION VS LAYOUT

The entire analysis is centered on a basic test structure that was fabricated in the standardized poly-MUMPs process. Properties are extracted by analyzing the effect of simple modifications to the design. It is assumed that the only run data provided is layer thickness h which is typically the only well-controlled process parameter. An optical image of the test structure is shown in Figure 1. The simplicity of the design allows properties to be more clearly targeted and increases the workability. Two SEM insets show magnified views of geometrical nonidealities such as "webbing" instead of sharp 90° corners at all beam-to-base interfaces, coarse sidewalls instead of smooth surfaces, beam widths which have recessed ~20%, and gaps which have increased ~20%. Base compliance in the plate and anchor, labeled as κ_{bc} in the figure, permits a planar

rotation of $\Delta\phi$ at the beam-to-base interface such that support beams do not meet the base at right angles upon bending. This effect is magnified by beam length. The webbing effect appears at all acute corners. Its presence at the interface between the support beams and the plate and anchor increases the apparent stiffness of the support beams by κ_{web}. Furthermore, enlarged gaps reduce capacitance and comb drive force; thinned beams reduce system stiffness; and residual stress offsets comb finger alignment. These effects are considered below.

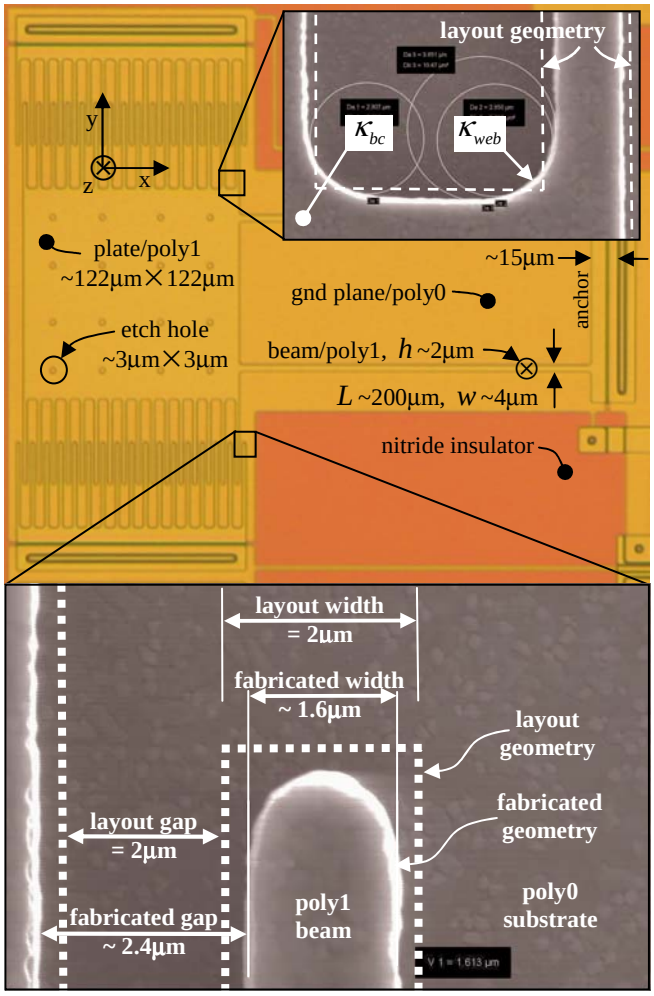

Figure 1: Basic test structure.

3 THEORY

If device components are fabricated within relative close proximity to each other and have the same orientation such that deposition, lithographic, and etchant reactions among corresponding components are alike, then it is safe to assume that material properties and geometric inaccuracies are locally consistent. We assume that small deflection theory applies such that the system can be effectively modeled as a 1D second order nonhomogeneous ODE with constant coefficients. However, we do not assume a parallel plate approximation for the comb drive.

3.1 Measuring planar geometry

We begin by extracting the fabrication error in beam width Δw, which we define as the difference between the layout width and the fabricated width. Let there be two test structures, a and b, of the type shown in Figure 1. Assume that all layout geometries are identical except for the widths of the parallel support beams. Let the layout beam widths of a and b differ by a multiplicative layout parameter n_b, such that $w_{b,layout} \equiv n_b w_{a,layout}$. We express the fabricated widths in terms of layout and error as,

$$w_a = w_{a,layout} + \Delta w, \text{ and } w_b = n_b w_{a,layout} + \Delta w. \quad (1)$$

The case of a rigid plate and anchor is considered first. If a potential ΔV_0 is applied to a and b, the balance of static equilibrium $F_{spring} = F_{electrostatic}$ is,

$$k_{eff,a}\Delta y_a = \frac{1}{2}\Delta V_0^2 \frac{\Delta C_a}{\Delta y_a}, \text{ and } k_{eff,b}\Delta y_b = \frac{1}{2}\Delta V_0^2 \frac{\Delta C_b}{\Delta y_b} \quad (2)$$

where k_{eff} is the effective stiffness, and ΔC is the linear change in capacitance of the comb drive due to a small lateral displacement Δy. Since a and b have identical comb drives, then their electrostatic forces are identical as well. Equating the expressions in (2) and taking their ratio to be unity, we find

$$\frac{\Delta C_a}{\Delta C_b} = \frac{w_b^3}{w_a^3} = \frac{\left(n_b w_{a,layout} + \Delta w_{eff}\right)^3}{\left(w_{a,layout} + \Delta w_{eff}\right)^3}, \quad (3)$$

where $k_{eff} \propto w^3$. Solving for the effective error, we have

$$\Delta w_{eff} = \left(\frac{n_b \left(\Delta C_b / \Delta C_a\right)^{1/3} - 1}{\left(\Delta C_b / \Delta C_a\right)^{1/3} - 1} \right) w_{a,layout}. \quad (4)$$

If compliancy in the plate and anchor is considered, then the effective stiffness can be dissected as

$$k_{eff} = k + 4\kappa \quad (5)$$

where k is the stiffness of the parallel beam supports (18), and κ is defined as $\kappa \equiv \kappa_{bc} w^2 + \kappa_{web}$ for each beam-to-base interface [13]. The additional unknowns κ_{bc} and κ_{web} require two additional test structures that differ from a and b in layout beam width only. Then by taking ratio combinations and equating forces, the quantities κ_{bc}, κ_{web}, and Δw, may be expressed solely in terms of changes in capacitance and layout geometry [13].

Although the effective error Δw_{eff} and the actual error Δw are fitted to match experiment, Δw_{eff} absorbs base compliancy, while Δw filters it out to capture the average width of the beam. Similar arguments apply to k_{eff} and k.

From the introductory assumptions, it can be inferred that the error in beam width identically applies to all planar

geometries as well. Such as the lengths of support beams, gaps, and cantilevers are respectively,

$$L = L_{layout} - \Delta w,\ g = g_{layout} - \Delta w, \text{ and } L_f = L_{f,layout} \quad (6)$$

where cantilevers are simply translated toward their base. The areas of rectangular plates and comb fingers are

$$A_{plate} = \left(L_{1,layout} + \Delta w\right)\left(L_{2,layout} + \Delta w\right) - N_H\left(L_H - \Delta w\right)^2,$$
$$A_{comb} = N_f L_{f,layout}\left(w_{layout} + \Delta w\right),\ A_{beam} = \left(L_{layout} - \Delta w\right)\left(w_{layout} + \Delta w\right) \quad (7)$$

where N_H and N_f are the numbers of holes and fingers. The fabricated geometry (6)-(7) with respect to error Δw is exemplified in Figure 2.

3.2 Measuring dynamic properties

Modifying the basic test structure to include displacement stops (labeled as ds in Figure 2) allows a precisely defined displacement to be obtained. Upon closure of this gap, the comb drives will be displaced by

$$\Delta y_{ds} = g_{layout} - \Delta w, \quad (8)$$

which corresponds to a change in capacitance of ΔC_{ds}.

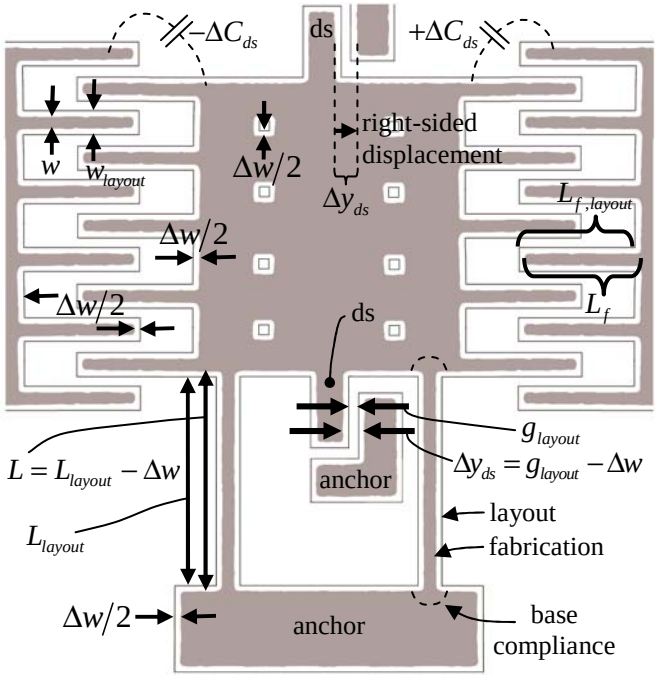

Figure 2: Fabricated geometry (solid) vs layout (outline)

The potential that is applied to close the gap will most likely be greater than what is necessary. The precise voltage required to displace Δy_{ds} may be obtained by reverse-biasing the system such that the structure deflects in the opposite direction, which is not limited by the displacement stop. Upon reaching an identical change in capacitance ΔC_{ds}, the potential that produces this change ΔV_{ds} corresponds to the prescribed deflection in (8). Hence, a measurement of the comb drive force is revealed as

$$F_0 = \frac{1}{2}\Delta V_{ds}^2 \frac{\Delta C_{ds}}{\left(g_{layout} - \Delta w\right)} \quad (9)$$

which includes comb finger misalignments and fringing field effects. Designers often estimate the comb drive force using the parallel plate approximation, $\alpha \frac{1}{2} V^2 N_f h / g_{layout}$, where $\alpha \approx 1.12$ is the fringing field correction factor. Using (9), α may be precisely measured as $\alpha = \Delta C_{ds} g_{layout} / N_f h \varepsilon_0 \left(g_{layout} - \Delta w\right)$.

Now let ΔV_{ds} be applied sinusoidally such that (9) is the amplitude of the driving force. Then the lumped-model equation of motion for the system is represented by

$$m_{eff}\ddot{y} + d_{eff}\dot{y} + k_{eff} y = F_0 e^{i\omega t}, \quad (10)$$

where d_{eff} includes damping of the plate, comb drives, and support beams, and ω is the frequency of the voltage source. It can be shown [13, 8] that the displacement and velocity amplitudes are maximized when the driving frequency equals the displacement and velocity resonance frequencies, ω_r and $\omega_0 = \sqrt{k_{eff}/m_{eff}}$ respectively. These resonances are related to the natural frequency ω_d by

$$\omega_r^2 = 2\omega_d^2 - \omega_0^2 \quad (11)$$

where $\omega_d^2 \equiv \omega_0^2 - \left(d_{eff}/2m_{eff}\right)^2$, $\omega_r^2 \equiv \omega_0^2 - 2\left(d_{eff}/2m_{eff}\right)^2$. Displacement resonance may be measured by maximizing the amplitude of the output signal of the capacitive divider as a function of frequency. Velocity resonance may be measured by maximizing the amplitude of the output signal of a capacitive divider that is sent through a differentiator as a function of frequency [13]. It is important to note that only the velocity resonance in (11) is independent of damping – even for critically damped systems. It is also shown that damping is related to the displacement amplitude y_0 and natural frequency by

$$d_{eff} = F_0 / y_0 \omega_d \quad (12)$$

where the displacement and velocity amplitudes are

$$y_0 = F_0 / 2\gamma m_{eff}\sqrt{\omega_0^2 - \gamma^2}, \text{ and } \dot{y}_0 = F_0 / 2\gamma m_{eff} \quad (13)$$

Realizing that (2), (9), (12), and (13) are expressions relating to the same force amplitude in (10), we measure the effective damping, mass, and stiffness as

$$d_{eff} = \frac{\Delta V_{ds}^2 \Delta C_0}{2 y_0^2 \omega_d},\ m_{eff} = \frac{d_{eff}}{2\gamma}, \text{ and } k_{eff} = m_{eff}\omega_0^2 \quad (14)$$

where the exponential damping factor is defined as $\gamma^2 \equiv \left(\omega_0^2 - \omega_r^2\right)/2$, and we have assumed that the ratio of the change in capacitance to displacement for over the linear range of the comb drive is the constant $\Delta C_0 / y_0 = \Delta C_{ds} / \Delta y_{ds}$. γ^{-1} is the time for which the amplitude of motion decays by a factor of e^{-1} once the driving force is removed.

3.3 Measuring material properties

Now that the geometric and dynamic properties have been determined, material density can be found by taking the ratio of the effective mass to the effective volume,

$$\rho = \frac{m_{eff}}{v_{eff}} = \frac{m_{eff}}{h\left(A_{plate} + A_{comb} + 2\times\frac{13}{35}A_{beam} \right)} \quad (15)$$

where geometry (7) and a Rayleigh-Ritz method [13] is used to find the effective volume of the system.

We define the quality factor of the system as

$$Q \equiv \frac{\omega_d}{\sqrt{\left(\omega_0^2 - \omega_r^2\right)/2}} = \frac{m_{eff}\,\omega_d}{d_{eff}}. \quad (16)$$

The Young's modulus of the material can be found by substituting geometry, k_{eff}, and κ into equation (5), [13]. By absorbing the effects of base compliance, an effective Young's modulus is more simply expressed as

$$E_{eff} = \frac{k_{eff}\left(L/2\right)^3}{3I} = \frac{k_{eff}\left(L_{layout} - \Delta w\right)^3}{2h\left(w_{a,layout} + \Delta w\right)^3}. \quad (17)$$

where I is the second moment of area of the fitted model.

Once Young's modulus is uncovered, we find the stiffness of the parallel beam supports to be

$$k = 2Eh\left[\left(w_{layout} + \Delta w\right)/\left(L_{layout} - \Delta w\right)\right]^3. \quad (18)$$

The shear modulus G is related to Poisson's ratio ν by $G \equiv E/2\left(1+\nu\right)$. Assuming small deflection theory applies, shear rotation at the beam-to-base interface is [13]

$$\Delta\phi = 4LF_0/\pi hGw_a^2 = \Delta y_{ds}/L \quad (19)$$

which leads us to a shear modulus and Poisson's ratio of,

$$G = \frac{4L^2F_0}{\pi h\Delta y_{ds}\left(w_{a,layout} + \Delta w\right)^2}, \text{ and } \nu = \frac{E}{2G} - 1. \quad (20)$$

Lastly, planar residual stress may be obtained by capacitively measuring the stress induced elongation of a beam. If the structure in Figure 1 is modified such that one comb drive is replaced with a beam that laterally extends for some length L_σ before it is anchored, then its change in length Δy_σ may be detected by a change in capacitance ΔC_σ in the remaining comb drive, where the unmodified test structure is the reference. Since the Δy_σ is related to capacitance and stress by $\Delta C_\sigma/\Delta y_\sigma = \Delta C_{ds}/\Delta y_{ds}$ and $\sigma = E\Delta y_\sigma/L_\sigma$, we write the stress and elongation as

$$\sigma = \frac{E\Delta y_{ds}\Delta C_\sigma}{\left(L_{\sigma,layout} - \Delta w\right)\Delta C_{ds}}, \text{ and } \Delta y_\sigma = \frac{\Delta C_\sigma}{\Delta C_{ds}}\Delta y_{ds}. \quad (21)$$

If planar stress is significant, then large geometric quantities in (6)-(7) must be adjusted accordingly.

4 CONCLUSION / FUTURE

Practical analysis techniques for measuring over a dozen MEMS properties have been proposed. Accuracy was addressed by formulating all properties in terms of precise electrical measurements and exactly known layout geometry. Confidence was addressed by uncovering the underlying dependencies. Possible benefits of these methods are as follows. Small test sets reduces chip real-estate costs and allows structures to be positioned alongside primary MEMS devices for localized testing. Electronic probing allows packaged testing to be performed in-the-field, such as monitoring the changes in properties due to the environment, fatigue, and recalibration after long-term dormancy. These methods may be applied to other designs.

Future work includes experimental verification, and the analysis of sensitivities and possible errors due to small deflection theory. Length and stress measurements will be verified by ASTM standards. The experimentally-accurate lumped models can be used in Sugar [13] and verified by comparing simulations to the performance of more complex designs on the chip. Measurements of other properties including nonlinear effects are being considered as well.

REFERENCES

[1] Small Times, "MEMS Standards, While Small, May Mean Much for the Industry," Aug 26, 2003

[2] J. Marshall, NIST, Gaithersburg, Md. www.astm.org/SNEWS/OCTOBER_2003/micro_oct03.html

[3] P. M. Osterberg, S. D. Senturia, "M-Test: A Test Chip for MEMS Material Property Measurement Using Electrostatically Actuated Test Structures," JMEMS, June 1997, v.6, no.2:107-118

[4] H. Guckel, et. al., "Diagnostic Microstructures for the Measurement of Intrinsic Strain in Thin Films," J. Micromech. and Microeng., 6 1992, v.2, no.2:86-95

[5] K. E. Peterson, et al., "Young's Modulus Measurements of Thin Films Using Micromechanics," J. Appl. Physics, 50, 1979, pp6761-6766.

[6] L. Lin, et. al., "A Micro Strain Gauge with Mechanical Amplifier" JMEMS, 6, 1997, pp313-321.

[7] W. Sharpe Jr., "Mechanical Properties of MEMS Materials" The MEMS Handbook, 2002, Ch3 pp1-33.

[8] G. R. Fowles, "Analytical Mechanics," Saunders, 1990

[9] S. D. Senturia, "Microsystem Design," Kluwer, 2001.

[10] M. Elwenspoek, R. J. Wiergerink, Mechanical Microsensors, Berlin, New York, Springer, 2001.

[11] R. K. Gupta, "Electronically Probed Measurements of MEMS Geometries," JMEMS v.9, no.3, 2000, p380.

[12] J. Green, et. al., "New iMEMS Angular Rate-Sensing Gyroscope," Analog Devices, Dialogue, 37-03, 2003.

[13] J. V. Clark, dissertation in progress, "Modeling, Simulation, and Design of Complex Microelectro-mechanical Systems," U.C. Berkeley, CA.